A measurement-based statistical model for industrial ultra-wideband channels

Kåredal, Johan; Wyne, Shurjeel; Almers, Peter; Tufvesson, Fredrik; Molisch, Andreas

Published in:
IEEE Transactions on Wireless Communications

DOI:
10.1109/TWC.2007.051050

2007

A Measurement-Based Statistical Model for Industrial Ultra-Wideband Channels

Johan Karedal, *Student Member, IEEE*, Shurjeel Wyne, *Student Member, IEEE*,
Peter Almers, *Student Member, IEEE*, Fredrik Tufvesson, *Member, IEEE*, and Andreas F. Molisch, *Fellow, IEEE*

***Abstract*— The results of three ultra-wideband (UWB) measurement campaigns conducted in two different industrial environments are presented. A frequency range of $3.1 - 10.6$ or $3.1 - 5.5$ GHz was measured using a vector network analyzer and a virtual array technique enabling the investigation of small-scale statistics. The results show that the energy arrives in clusters, and that the abundance of metallic scatterers present in the factory hall causes dense multipath scattering. The latter produces a small-scale fading that is mostly Rayleigh distributed; the only exception being the delay bin containing the line-of-sight component. The power delay profile can be modeled by a generalized Saleh-Valenzuela model, where different clusters have different ray power decay constants. It is also noted that the number of multipath components required to capture a majority of the energy is quite large. More than a hundred components can be needed to capture 50% of the total available energy.**

***Index Terms*— Ultra-wideband, channel measurements, statistical model, industrial environment.**

I. Introduction

IN recent years, ultra-wideband (UWB) spread spectrum techniques have gained increasing interest [1], [2], [3], [4]. UWB systems are often defined as systems that have a relative bandwidth larger than 20% and/or absolute bandwidth of more than 500 MHz [5]. There are several qualities of UWB systems that can be of interest in the area of wireless communications. The large relative bandwidth, as well as the large absolute bandwidth, ensures resistance to frequency-selective fading, which implies more reliable communications [6], [7], [8]. Also, the spreading of the information over a very large frequency range decreases the spectral density. This decreases interference to existing systems (which is important for commercial applications) and makes interception of communication more difficult (which is of interest for military communications). Finally, the concept of impulse radio allows the construction of communications systems with simplified transceiver structures [3], [6].

UWB communications are envisioned for a number of applications and there are two major trends in the development of new systems. The first is high-data rate communications, with data rates in excess of 100 Mbit/s [9]. One typical application for such a high-rate system is high-definition TV transmission. The other trend is data rates below 1 Mbit/s, usually in the context of sensor networks, and in conjunction with UWB positioning systems. A considerable part of these systems will be deployed in industrial environments. Interesting applications include machine-to-machine communications in e.g., process control systems, or supervision of storage halls.

For the planning and design of any wireless system, channel measurements and modeling are a basic necessity [10]. Previous UWB measurement campaigns have been restricted to office and residential environments, and there exist channel models for those environments, see e.g., [11], [12], [13], [14]. However, industrial environments have unique propagation properties (large number of metallic objects, dimensions of halls and objects) and thus existing UWB channel models, especially, the standardized IEEE 802.15.3a model [15], are not valid there. On the other hand, available *narrowband* channel models in industrial environments (e.g., [16]) cannot be used, because the behavior of the narrowband and the UWB channel is remarkably different as have been shown by numerous theoretical as well as practical investigations [11], [13], [14], [17], [18], [19], [20]. For these reasons, there is an urgent need for measurements of the UWB channel in industrial environments, and a subsequent channel model. To our knowledge, no such investigation has been published yet.

In this paper, we present results from three UWB measurement campaigns that cover the FCC-approved frequency band [5] (measurement campaign three only covers $3.1 - 5.5$ GHz) conducted in two industrial halls. We propose a statistical model for the measured data suitable as a basis for system simulations. It should be noted, however, that since the number of different factory halls we measure is limited, we do not claim our model to describe any "general" industrial environment. They best agreement between model and measurement can obviously be expected in halls very similar to the ones where our measurements were performed. Also, the outcome of the first measurement campaign has been used as input to the channel modeling group of IEEE 802.15.4a [21].

The remainder of the paper is organized the following way: Section II gives the details of the measurement setup. In Section III, we describe the measurement environment and transmitter and receiver locations, while Section IV covers the data processing. Section V presents results for the multipath propagation, clustering, and delay spreads and Section VI gives a statistical model based on our measurements. Finally, a summary and conclusions about UWB system behavior in

Manuscript received December 21, 2005; revised July 18, 2006; accepted August 17, 2006. The associate editor coordinating the review of this paper and approving it for publication was R. M. Buehrer. Parts of this work have been published at Globecom 2004, VTC 2004 Fall, and WPMC 2005.

J. Karedal, S. Wyne, P. Almers, and F. Tufvesson are with the Department of Electroscience, Lund University, Lund, Sweden (e-mail: {Johan.Karedal, Shurjeel.Wyne, Peter.Almers, Fredrik.Tufvesson@es.lth.se).

A. F. Molisch is with Mitsubishi Electric Research Labs, Cambridge, MA and also at the Department of Electroscience, Lund University, Lund, Sweden (e-mail: Andreas.Molisch@ieee.org).

Digital Object Identifier 10.1109/TWC.2007.051050.

TABLE I
MEASUREMENT SETUP PARAMETERS

	Campaign No.		
	1	2	3
Frequency range [GHz]	3.1 − 10.6	3.1 − 10.6	3.1 − 5.5
Frequency points	1251	1601	981
Delay resolution [ns]	0.13	0.13	0.42
Max. resolvable delay [ns]	167	213	408
Element separation [mm]	50	37	50

the measured environment is presented in Section VII.

II. Measurement Setup

The measurement data were acquired during three measurement campaigns. All measurements were performed in the frequency domain using a vector network analyzer (HP 8720C in the first two campaigns, Rohde&Schwartz ZVC in the third), determining the complex channel transfer function $H(f)$. In the first two campaigns, the measured frequency range was 3.1 to 10.6 GHz which implies a delay resolution of approximately 0.13 ns (corresponding to 4 cm path resolution). The difference between the two campaigns was the number of frequency points used. In the first campaign, the spectrum was divided into 1251 frequency points, i.e., 6 MHz between the frequency samples and thus a maximum resolvable delay (with the inverse Fourier transform technique that we use in this paper) of 167 ns (corresponding to 50 m path delay). In the second campaign, 1601 frequency points were used, implying a frequency resolution of 4.7 MHz and a maximum resolvable delay of 213 ns (64 m path delay). The third measurement campaign limited the measured frequency range to 3.1 to 5.5 GHz, giving a delay resolution of 0.42 ns. 981 frequency points were used, giving a maximum resolvable delay of 408 ns (122 m path delay).[1] All measurement parameters are summarized in Table I.

Omnidirectional conical monopole antennas (Antenna Research Associates, Model No. CMA-112/A) were used as transmitter as well as receiver throughout all three campaigns. Using stepper motors, the monopoles were moved to different positions along rails, thus creating a *virtual* uniform linear antenna array (ULA) at each end (for a picture of the full setup, see [22]). In the first and the third campaign, the separation between the array elements was set to 50 mm, which corresponds to $\lambda/2$ at 3.1 GHz. In the second, the array element separation was 37 mm ($\lambda/2$ at 4 GHz). By moving each antenna, a virtual MIMO system of 7 by 7 antennas was created. Each rail was mounted on a tripod, with a height of 1.0 m, and moved to various locations in the building.

III. Measurement Environment

A. Measurement Campaign 1 and 2: DSM Resins Scandinavia

The first two measurement campaigns were performed in a factory hall in Landskrona, Skåne, Sweden. The hall was an incinerator hall of DSM Resins Scandinavia, a chemical company producing resins for coating systems. The hall has

[1]This campaign was actually measured over a frequency range 3.1 − 8.0 GHz, but all resulting frequency responses displayed several strong peaks for the higher frequencies, probably due to interference from the equipment in the hall, and hence only the lowest 2.4 GHz was used in the analysis.

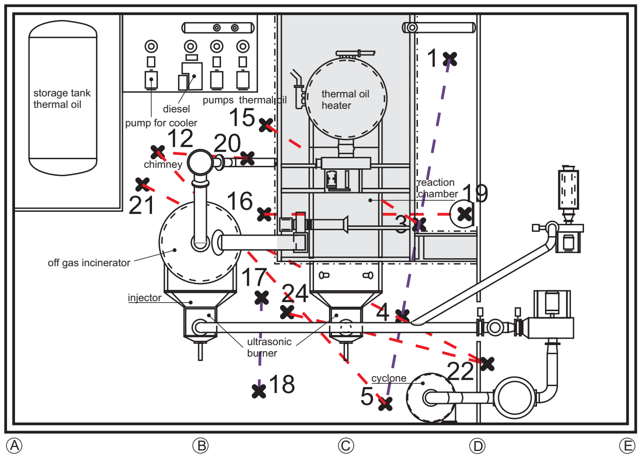

Fig. 1. The incinerator hall of DSM Resins as seen from above. The numbers indicate different antenna positions and the dashed lines show between which positions measurements were made.

Fig. 2. An inside view of the incinerator hall at DSM Resins. The photograph is taken from the position corresponding to the lower left corner of Fig. 1, showing the cyclone next to antenna position 5 at the rightmost of the picture.

a floor area of 13.6 × 9.1 m and a height of 8.2 m (see Fig. 1). Comparing this with the maximum path delay (see Section II) it can be noted that the latter is about four or five times the largest dimension of the building (for the first and second measurement campaign, respectively). The walls and ceiling of the factory hall consist mostly of metal (corrugated iron), whereas the floor is made of concrete. In addition to the metallic walls and ceiling, the building is also packed with metallic equipment, e.g., pumps, tanks and pipes (see Fig. 2). At one end of the building, there is a balcony (between points D to E in Fig. 1) at 3 m height. From the balcony, a metal grate bridge stretches into the room (the shaded area in Fig. 1), covering positions over the reaction chamber.

Inside the building, positions were selected to obtain three different scenarios, as well as three different transmitter - receiver separations. The different scenarios were: line-of-sight (LOS), peer-to-peer non-line-of-sight (PP NLOS) and base station (BS) NLOS. In the BS NLOS scenario, the transmitter array tripod was placed on top of the balcony (position 22 in Fig. 1) while the receiver array remained on floor level. For the LOS and PP NLOS scenarios, three different antenna separations were measured, 2 m, 4 m and 8 m, whereas for the BS NLOS only two separations, 5 m and 9 m (horizontal distance), were used. Campaign one included three LOS measurements, all performed along the same line, alongside the reaction chamber, and five NLOS measurements (3 PP and 2 BS), where transmitter and receiver were separated by the reaction chamber and/or the parts of the incinerator. Campaign two included one LOS measurement and two PP NLOS measurements.

The antenna arrays were aimed to be aligned broadside to broadside, and hence parallel. However, for practical reasons achieving perfect aligning of the arrays was very difficult, especially for the NLOS measurements when often no points of reference could be used to assure a proper alignment.

There was no moving machinery inside the incinerator hall during the measurements, and no moving personnel. Thus, the measurement environment was stationary, a basic requirement for the measurement technique used here.

B. Measurement Campaign 3: MAX-Lab

The third measurement campaign was performed in MAX-Lab, a medium-sized industrial environment in Lund, Sweden. The hall has a floor area of 94×70 m and a ceiling height of 10 m. This hall has walls made of reinforced brick and concrete, a ceiling made of steel and a floor made of concrete. Since it also contains many metallic objects, e.g., pipes, pumps and cylinders, it too constitutes a rich scattering environment.

Inside the factory hall, 16 receive antenna positions for PP NLOS measurements, spread over 4 different Tx positions, were selected along with 6 receive antenna positions for BS NLOS, spread over 2 Tx positions. In the BS NLOS measurements, the Tx antenna was elevated 3 m above floor level. The measured Tx-Rx separations for PP NLOS were 2, 3, 4, 6, 8, 10, 12 and 16 m, whereas separations of 4, 8, and 12 m (horizontal distance) were used in the BS NLOS measurements.

IV. Measurement Data Processing

The measured transfer functions were processed the following way: the transfer function between the mth transmit and nth receive antenna position within the virtual arrays, $H(f, m, n)$, was inverse Fourier transformed (applying a Hanning window to suppress aliasing) to the delay domain, resulting in the impulse response $h(\tau, m, n)$.[2] From that, we define the instantaneous power delay profile (PDP) as the square magnitude of the impulse response, i.e.,

$$\mathrm{PDP}(\tau, m, n) = |h(\tau, m, n)|^2 \quad (1)$$

For each 7×7-measurement the 49 corresponding instantaneous PDPs were averaged to obtain the averaged PDP (APDP) as

$$\mathrm{APDP}(\tau) = \frac{1}{MN} \sum_{m=1}^{M} \sum_{n=1}^{N} PDP(\tau, m, n) \quad (2)$$

where M and N are the number of receive and transmit elements, respectively.

[2]Note that a small amount of aliasing is still present in some of our measurements, see, e.g., Fig. 5.

The method of spatial averaging is classical, but when used in conjunction with UWB it gives rise to some concerns. A multipath component that will arrive at a certain delay τ_i when received by antenna array element 1, will arrive a time increment $\Delta\tau$ later when received by antenna element 2. Due to the fine delay resolution, τ_i and $\tau_i + \Delta\tau$ may fall into different delay bins. In that case, the averaging will have a "smearing" effect, as what really should be present in only one delay bin instead will be represented in several.

In [11], it has been suggested to adjust the delay axis of the power delay profile so that the (quasi)-LOS component of all instantaneous PDPs of the same measurement corresponds to the same delay bin (the required adjustment can be obtained from simple geometrical considerations). Such a correction facilitates a more accurate extraction of the statistical parameters of the first arriving component. However, due to the array aligning and the maximum possible excess runtimes, this effect is not significant in our measurement setup for the LOS component. For later arriving components, no delay adjustment has been made either, since without accurate angular information for each MPC, such a procedure is not possible.

The concerns connected spatial averaging also affects the rms delay spread since, by definition, the delay spread is based on the APDP. However, since the rms delay spread is such a widely used parameter for a wireless channel, we included the results in our analysis. The rms delay spread is defined as the second central moment of the APDP [23]

$$S(\tau) = \sqrt{\frac{\int_{-\infty}^{\infty} \mathrm{APDP}(\tau)\tau^2 d\tau}{\int_{-\infty}^{\infty} \mathrm{APDP}(\tau) d\tau} - \left(\frac{\int_{-\infty}^{\infty} \mathrm{APDP}(\tau)\tau d\tau}{\int_{-\infty}^{\infty} \mathrm{APDP}(\tau) d\tau} \right)^2} \quad (3)$$

V. Results

In this section, we analyze the measurement results, and draw conclusions about propagation effects. We will pay special attention to those effects that are specifically caused either by the industrial environment (multiple metallic reflectors) and/or the very large bandwidth of the measurements.

A. Power Delay Profiles

A first effect we can observe is that the APDPs consist of several distinct clusters, which are clearly identifiable even with the naked eye (see Fig. 3). This clustering of multipath components (MPCs) has also been observed in indoor office and indoor residential environments (both for the narrowband and the ultra-wideband case) and can be modeled by the Saleh-Valenzuela (SV) model [13], [14], [18], [19], [20], [21]. However, inspection of Fig. 3 reveals two important differences to the conventional SV model:

1) The decay time constants of the different clusters are different. Typically, clusters with a longer delay exhibit a larger decay time constant.
2) The clusters do not necessarily show a single-exponential decay. In some cases, they can be better described as the sum of a discrete (specular) component and a "diffuse" cluster with a longer decay time constant (see, e.g., the third cluster in the upper APDP of Fig. 3).

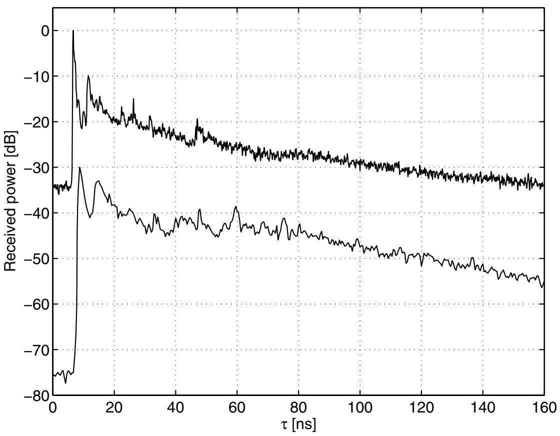

Fig. 3. Average power delay profiles for 2 m LOS (DSM Resins; upper curve) and 2 m PP NLOS (MAX-Lab; lower curve) normalized to their strongest component. The latter is plotted with a −30 dB offset.

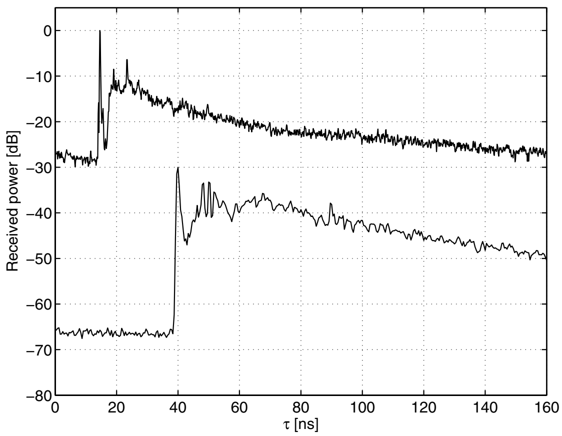

Fig. 4. Average power delay profiles for 4 m PP NLOS (DSM Resins; upper curve) and 12 m BS NLOS (MAX-Lab; lower curve) normalized to their strongest component. The latter is plotted with a −30 dB offset.

For the LOS components, as well as most NLOS situations, the first component is strong and followed by a pronounced minimum in the APDP. A similar effect has also been observed in office environments [18]. A possible interpretation for this minimum is that the Fresnel ellipsoid that corresponds to a delay of one bin (130 ps) is free of scatterers. Alternatively, the minimum is created by the "smearing" effect caused by the spatial averaging, since this effect is less pronounced for MPCs entering from broadside direction, such as the LOS component.

Another important observation in that context is that the first arriving component is very strong even in NLOS situations when the distance between Tx and Rx is small (see lower APDP of Fig. 3 and upper APDP of Fig. 4). A 4 m PP NLOS measurement was performed in measurement campaign 1, with the antennas separated by the large reaction chamber (Tx at position 19, Rx at position 16), i.e., LOS was definitely blocked. But even for this location that was so clearly NLOS, the effective behavior of the impulse response very much resembles the LOS measurements. Also, the rms delay spread value, 34 ns, of this measurement resembles the LOS results (e.g., the 4 m LOS has a mean rms delay spread of 31 ns) rather than the other NLOS measurements. Using a conventional beamformer [24] on the lowest 0.9 GHz sub-band $(3.1 - 4.0\ \text{GHz})$[3] for the upper APDP in Fig. 4 reveals that each of the two main peaks has an angle-of-arrival as well as an angle-of-departure that is almost broadside. Considering the delay times of these bins, one can by inspection of the map identify these paths. The first peak belongs to the path below the reaction chamber, reflected only by the floor, and the second is the path above the chamber, reflected by the metal grate on the balcony.

The measurements discussed above show a behavior that is somewhat similar to the classical exponential decay, i.e., the first arriving component is the strongest, and the APDP (or at least the envelopes of the multiple clusters) decays more or less monotonically. However, this situation changes drastically for NLOS situations with larger Tx-Rx separations, as depicted in Fig. 5. There, we observe that the maximum of the APDP occurs some 10-40 ns *after* the arrival of the first multi-path component (MPC); the power after this maximum is monotonically decreasing. This shape of the APDP can have significant impact on the system performance, as discussed in Section VII.

[3]Since the main focus of this paper was not angular information, the antenna element separation of the virtual arrays was not selected to allow for an analysis of the whole frequency spectrum. The conventional beamformer may result in angular ambiguities when the antenna separation is larger than $\lambda/2$ and hence, only a low frequency sub-band was used in the analysis.

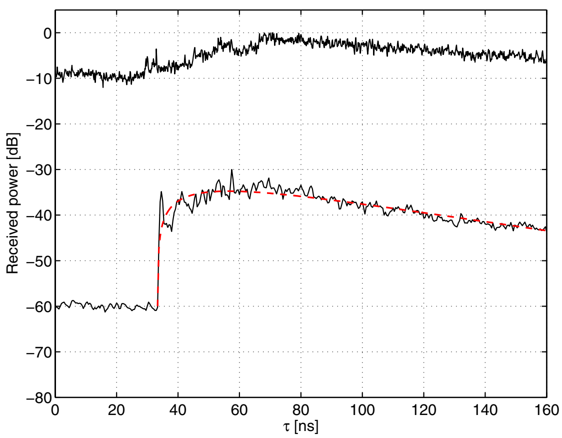

Fig. 5. Average power delay profiles for 8 m PP NLOS (DSM Resins; upper curve) and 10 m PP NLOS (MAX-Lab; lower curve) normalized to their strongest component. The latter is plotted with a −30 dB offset. The dashed curve shows a fit to Eq. (9).

Since these two types of APDP shapes are present in the results from both measurement sites, it seems reasonable to divide the analysis of the NLOS results into two groups, NLOS A and NLOS B. The NLOS A group contains measurements for shorter distances. These have a strong first component and a general shape very similar to the LOS cases. The NLOS B group contains measurements for larger distances, and these all have a "soft onset", i.e., a power that is not monotonically decreasing with delay. For DSM Resins, PP NLOS measurements over distances less than 8 m belong to NLOS A, while for MAX-Lab PP NLOS measurements over

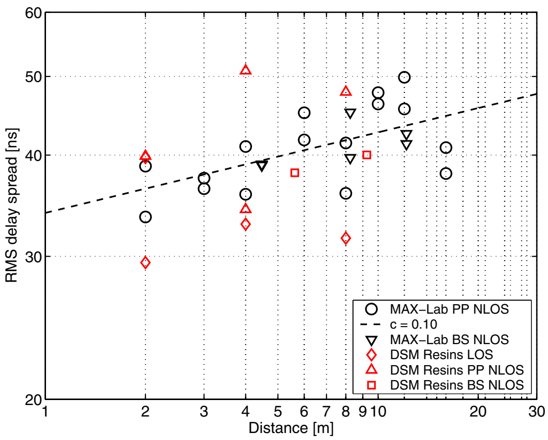

Fig. 6. Rms delay spread for all measurements. The dashed line ($c = 0.1$) corresponds to a best-fit to Eq. (4) for the MAX-Lab PP NLOS measurements.

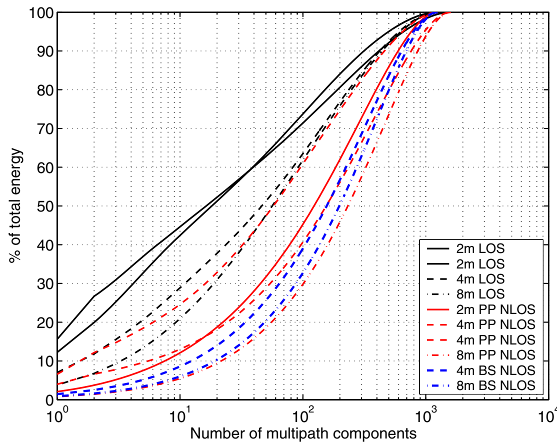

Fig. 7. The received energy for a certain number of multipath components for the measurements at DSM Resins.

distances less than 10 m belong to the same group.

Regarding the BS NLOS measurements, the APDP shape differs between the two sites. For DSM Resins, though it is hard to draw any general conclusions as only two BS measurement were made there, the APDP has a "soft onset" as in the case of the NLOS B discussion above. For MAX-Lab, however, the APDP shape agrees with shorter range measurements, i.e., they have a strong first component, even for the largest measured distance, 12 m (see lower APDP of Fig. 4). Hence, these are treated as NLOS A.

B. Delay Spread

As a further step, we analyze the rms delay spread in our measurements. For measurement campaign 1 and 2, the mean rms delay spread, as defined by Eq. 3, ranges from 28 ns to 38 ns for the LOS measurements, and from 34 ns to 51 ns for the NLOS measurement (PP and BS included). For measurement campaign 3, the rms delay spread varies between 34 ns to 50 ns for PP NLOS and between 39 ns and 45 ns for BS NLOS. For comparison, consider the narrowband measurements of [16] in an industrial environment: here, the rms delay spreads vary between 25 and 150 ns for both LOS and NLOS (there called OBS; obstructed); however, we note that the physical dimensions of some of those factory halls were larger than in our case.

The rms delay spread has often been reported to increase with distance [25]. This is also the case in our measurements. In Fig. 6 the rms delay spread is plotted as a function of distance for all measurements. Thus, we model the distance dependence with a power law as

$$\tau_{rms} \propto d^c. \quad (4)$$

Only the MAX-Lab PP NLOS scenario (represented by the circle markers in Fig. 6) has a number of measurements that is large enough to allow an extraction of the constant c, which in this case is 0.10.

For the design of Rake receiver systems, it is important to know the number of MPCs to be collected in order to capture a certain amount of the energy. Our analysis shows the difficulty of designing a Rake receiver for an industrial environment. For distances of 8 m in a NLOS scenario, collecting the 100 strongest MPCs would still only capture a little more than 30% of the total energy (see Fig. 7). This demonstrates the challenges of designing UWB systems in industrial environments.

VI. Statistical Model

In this section we give a statistical model that fits the measured data. As mentioned in Section V, our measured data show several clearly identifiable clusters in the APDPs, hence following the SV model seems reasonable. The SV model is widely accepted, simple and has also been adopted by the modeling group of IEEE 802.15.4a, where measurement campaign 1 of this paper was used as input. However, since then measurement campaign 2 and 3 has been conducted, and the combined result from all three measurement campaigns has given rise to some questions whether the power decay of the SV model being the best description. Hence, we also give a brief description on an alternative way of modeling the power decay in Section VI-B.

A. The Saleh-Valenzuela Model

The Saleh-Valenzuela (SV) model is commonly used to describe multi-cluster impulse responses, since its basic assumption is that multipath components arrive in clusters. In the SV model, the impulse response is given by

$$h(t) = \sum_{l=0}^{\infty} \sum_{k=0}^{\infty} \beta_{kl} e^{j\theta_{kl}} \delta(t - T_l - \tau_{kl}), \quad (5)$$

where β_{kl} and θ_{kl} are the gain and phase of the kth ray of the lth cluster, respectively, whereas T_l is the arrival time of the lth cluster and τ_{kl} the arrival time of the kth ray measured from the beginning of the lth cluster. The gain is determined by

$$\overline{\beta_{kl}^2} \equiv \overline{\beta^2(T_l, \tau_{kl})} = \overline{\beta^2(0,0)} e^{-T_l/\Gamma} e^{-\tau_{kl}/\gamma}, \quad (6)$$

where Γ and γ are the cluster and ray power decay constants, respectively [26].

Thus, to describe our measured data we need the following: Cluster arrival rate, ray arrival rate, cluster power decay and ray power decay. Note that the concept of cluster and ray power decay is only meaningful for LOS measurements and NLOS A measurements. The corresponding NLOS B analysis is covered in Section VI-A.5.

Our first objective is to divide each APDP into clusters. The identification can be performed in several ways: when the clusters are well-separated in the delay domain, it is sufficient to find the maxima of the power delay profile, since these signify the onset of a new cluster. Alternatively, a "best fit" procedure can be used, where the number and start time of clusters are used as parameters that are fitted to the measured power delay profile. This approach was used, e.g., in the parameterization of the IEEE 802.15.3a channel models. However, it can suffer from numerical problems - depending on the choice of the start values of the minimum-search algorithm, different solutions (that all fit the measurement results) can be obtained. It should be noted that, at the moment, there is no formal way of identifying clusters. We thus in this paper choose an approach "by visual inspection" [27], [28], as the human eye is good at the detection of patterns and structures even in noisy data.

To identify different clusters, we make use of two criteria: (i) the observation from Section V-A, that different clusters have different decay time constants, and (ii) that the onset of a new cluster most often is marked by a pronounced step in receive power. Hence, we can focus on identifying pronounced steps in conjunction with different slopes in our APDPs. The first criterion is used, so that, when stepping along the delay axis, a cluster contains all delay bins that can be described reasonably good by the same, fitted, regression line. Exceptions to this procedure occur when there is one strong (specular) component followed by some diffuse clutter, since the specular component is not that well described by a "decay of its own". In these cases, the specular component and the clutter are included in the same cluster. Generally, in all our measurements we have a number of clusters that ranges between 4 and 6. On average, 5 clusters are observed.

While the number of impulse responses used for estimation does affect the appearance of the APDP, we note that this number has no significant effect on our cluster identification. This, of course, unless more measurements from a *much larger* geometric area (i.e., using longer virtual arrays) are combined, as this would enhance the smoothing effect discussed in Section IV. Comparing APDPs derived from 25 measurements, with APDPs derived from 49 measurements, the clusters can be seen to be essentially the same.

1) Cluster Arrival Rate: The cluster arrival rate Λ is obtained by measuring the cluster interarrival times $\Delta T_l = T_l - T_{l-1}$ for each APDP, with $\Lambda = 1/\overline{\Delta T_l}$ where $\overline{\Delta T_l}$ is the average value within the APDP. We note that ΔT_l seems to increase with delay in our measurements. However, this is not used any further, since the number of measured T_l (which are *realizations* of a random variable) is not sufficient to allow determination of a general trend for the probability density function. According to the SV model, ΔT_l is described by an exponential distribution and this agrees well with our results (see Fig. 8). All values are given in Table II.

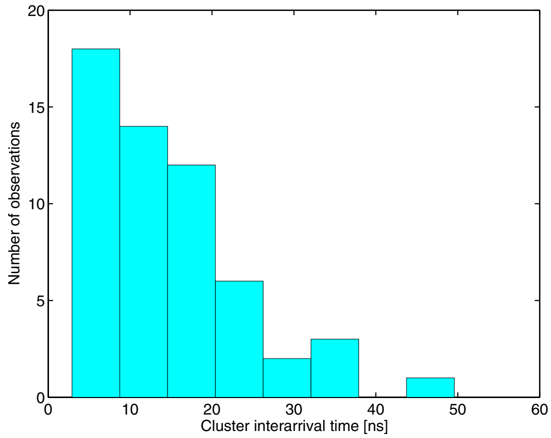

Fig. 8. A histogram of the cluster interarrival times for all measurement points from the measurements at MAX-Lab.

2) Ray Arrival Rate: The ray arrival rate λ is not determined since, despite the fine delay resolution (at best 0.13 ns, for measurement campaign 1), it was not possible to resolve the inter-path arrival times by an inverse Fourier transform of the measured data. Each resolvable delay bin contains significant energy. Therefore, we use a tapped delay line approach in our model, i.e., let every delay tap (on the measurement grid) contain energy according to Eq. (6).

3) Ray Power Decay: The standard SV model assumes that the γ:s are the same for all clusters of a certain impulse response. As previously mentioned, this is not the case in our measurements. The identification process of above immediately gives the ray power decay constant γ_l of each cluster as

$$\gamma_l = \frac{10}{k_{reg,l} \ln 10}, \tag{7}$$

where $k_{reg,l}$ is the negative slope of the regression line (on a dB-scale) belonging to cluster l and $\ln\{\sim\}$ is the natural logarithm. The γ values range from 0.5 to 70 ns, and since there are large differences of the values within a measurement, an average value is not a sufficient way of describing them. Generally, γ increases with delay, where the delay of a cluster l is defined as the arrival time of the first component of that very cluster, i.e., T_l in Eq. (5).[4] We thus propose a generalized SV model where γ increases linearly with delay (see Fig. 9), i.e.,

$$\gamma = \gamma(\tau) = \gamma_0 + a\tau, \tag{8}$$

where γ_0 is the ray power decay constant of the first cluster. This gives values of the constant a in the range of $0.5 - 1.2$ (see Table II).

4) Cluster Power Decay: The cluster power decay constant Γ is determined as the exponential decay of the peak power of the received clusters. To derive parameter values, we first normalize all (linear) cluster peak power values for each APDP so that the first cluster starts at 1. Then, all peak powers belonging to the same measurement site and scenario (e.g., PP

[4]Indeed, there are a few cases where some uncertainty remains regarding exactly when one cluster ends and the next one begins, but this has only a minor effect on our results.

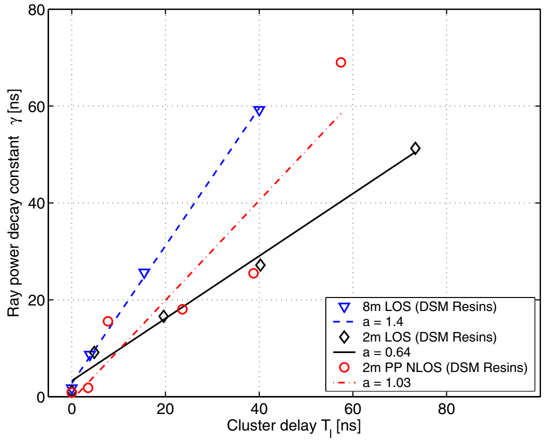

Fig. 9. Example plot of the linear delay dependence of the ray power decay constant γ. The figure shows γ as a function of delay for three different measurement positions from measurement campaign 1.

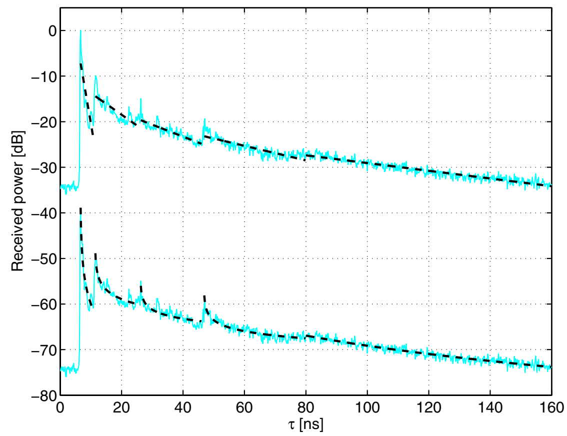

Fig. 10. A comparison of the classical SV model, i.e., an exponential power decay (upper curve), versus a power law decay (lower curve, plotted with a -40 dB offset) applied on the APDP of a 2m LOS measurement (DSM Resins). The upper curve has a mean square error (MSE) between measurement and model of $6.9 \cdot 10^{-4}$ whereas the lower curve has an MSE of $1.2 \cdot 10^{-4}$.

TABLE II

SALEH-VALENZUELA MODEL PARAMETERS

DSM	$1/\Lambda$ [ns]	Γ [ns]	γ_0 [ns]	a	γ_1 [ns]	γ_{rise} [ns]	χ
los	15.83	12.62	3.52	0.80	-	-	-
pp nlos a	13.10	29.78	4.13	1.19	-	-	-
pp nlos b	-	-	-	-	66.86	100	0.98
bs nlos (b)	-	-	-	-	71.36	11.12	0.90
MAX-Lab							
pp nlos a	16.00	28.87	4.98	0.54	-	-	-
pp nlos b	-	-	-	-	44.00	14.29	1.00
bs nlos (a)	12.53	24.01	2.53	0.69	-	-	-

NLOS) are plotted on a dB-scale as a function of the excess delay, and, finally, Γ is determined from a best-fit regression line in the same way as the ray power decay constant. This gives cluster power decay values in the range of $13 - 30$ ns (see Table II).

5) PDP Shape for NLOS B: As mentioned in Section V, the power of the measurements characterized as NLOS B is not monotonically decreasing, but there is a soft onset starting at the first arriving MPC where the power is actually increasing with delay. Hence, the power gains can no longer be described by Eq. (6). Instead, the power delay dependence is given by

$$\overline{\beta_{kl}^2} = \Omega_1 \frac{\gamma_1 + \gamma_{\text{rise}}}{\gamma_1 \left(\gamma_1 + \gamma_{\text{rise}} \left(1 - \chi\right)\right)} \left(1 - \chi e^{-\tau/\gamma_{\text{rise}}}\right) e^{-\tau/\gamma_1}, \tag{9}$$

where γ_1, γ_{rise} and χ are shape parameters while Ω_1 is the normalized power [21]. An example plot of the curve fitting of Eq. (9) is shown in Fig. 5. All parameter values are found in Table II.

B. Alternative Model - Power Law Approach

As previously mentioned, the SV model is commonly used, but it provides a fit to our data that is not entirely satisfactory. By mere inspection of the APDPs, it can be noted that the power decay of neither cluster, nor ray power is purely exponential (see Fig. 3). The ray power decay rather seems to follow a power law, i.e., the power within a cluster l is given by

$$P_{kl}\left(\tau_{kl}\right) = P_{0,l} \tau_{kl}^{-\alpha}, \tag{10}$$

where τ_{kl} is the arrival time of the kth ray measured from the beginning of the lth cluster. The power law decay has also been observed and discussed in [29], but then only for a single-cluster scenario. For our measurements, also the cluster peak power can be well described by a power law.

By visual inspection (see Fig. 10) the power law decay gives a better fit than the classical SV exponential decay. Results on this power law approach is reported in [30].

C. Small-Scale Statistics

For an indoor channel, many UWB measurement campaigns have reported an amplitude fading that follows a log-normal distribution (see e.g., [15]) or an m-Nakagami distribution (see e.g., [11]). Since these two distributions are the most frequently reported, we seek to analyze which of them that gives a better fit to our measured data, i.e., for each delay bin we investigate whether our observed amplitude vector $\mathbf{A} = \left[\begin{array}{cccc} A_1 & A_2 & \ldots & A_N \end{array}\right]$, where $N = 49$, has been drawn from an log-normal distribution or a m-Nakagami distribution. First, we turn our attention to the possibility of the latter, where m-parameter estimates are determined using the inverse normalized variance (INV) estimator [31]

$$\hat{m}_{INV} = \frac{\mu_2^2}{\mu_4 - \mu_2^2}, \tag{11}$$

where $\mu_k = N^{-1} \sum_{i=1}^{N} A_i^k$. It appears that for most of the measurements, an m-parameter estimate of 1 is achieved, which corresponds to a Rayleigh distribution. The only exception is for the delay bin containing the LOS component and a few adjacent delay bins. This is clearly different from the office environment in [11], where the m-parameter is found to be decreasing with the delay. Hence, the selection between log-normal and m-Nakagami changes to one between log-normal and Rayleigh.

Thus, for each delay bin we want to decide whether $\mathbf{A}$ was drawn from an Rayleigh distribution with a pdf

$p(\mathbf{A}; \hat{\sigma}_R, \text{Rayleigh})$, where $\hat{\sigma}_R$ is the maximum likelihood estimate (MLE) of σ_R given by

$$\hat{\sigma}_R = \sqrt{\frac{1}{2N}\sum_{i=1}^{N} A_i^2}, \tag{12}$$

or if $\mathbf{A}$ has been drawn from a log-normal distribution with a pdf $p(\mathbf{A}; \hat{\mu}_{LN}, \hat{\sigma}_{LN}, \text{log-normal})$, where $\hat{\mu}_{LN}$ and $\hat{\sigma}_{LN}$ are the MLEs of μ and σ given by the mean and standard deviation of $\ln\{\mathbf{A}\}$, respectively.

To make a choice between the two candidate distributions, we perform a generalized likelihood ratio test (GLRT) that decides, without favoring any of the two distributions, a Rayleigh distribution being the most likely if

$$\frac{p(\mathbf{A}; \hat{\sigma}_R, \text{Rayleigh})}{p(\mathbf{A}; \hat{\mu}_{LN}, \hat{\sigma}_{LN}, \text{log-normal})} > 1. \tag{13}$$

The result of the GLRT is that a Rayleigh distribution is more probably in more than 80% of the (excess) delay bins for each measurement. Hence, our model assumes that a Rayleigh distribution is applicable at all delays except for the LOS component. However, in order to avoid having to use different distributions for different delay bins, a more practical solution is to apply an m-Nakagami distribution to all delay bins, with an m-value of 1 used for all delay bins except the one containing the LOS component.

Several other tests have also been made in order to verify the result: (*i*) a Kolmogorov-Smirnoff test, (*ii*) a comparison of the mean square error between on one hand the cdf:s of a Rayleigh distribution and the measured data, and on the other the cdf:s a log-normal distribution and the measured data, (*iii*) a comparison of the Kullback-Leibler (KL) distance between a Rayleigh distribution and the measured data versus the KL distance between a log-normal distribution and the measured data. All of these tests have a few weaknesses, but regardless of these, all tests point towards a Rayleigh distribution.

The Rayleigh fading amplitude is a somewhat surprising result since it has been assumed that the fine resolution of the UWB would imply a too small number of paths arriving in each delay bin to fulfil the central limit theorem (CLT). A possible explanation why Rayleigh fading is yet observed here is that the high density of scatterers of the industrial environment creates a number of paths that is high enough to fulfil the CLT. An alternative explanation is that the problems of spatial averaging described in Section IV causes the Rayleigh distribution, i.e., the 49 values constituting the statistical ensemble for a certain delay bin may not be samples of the same MPC, but instead samples of several *different* MPCs.

D. Pathloss

The distance dependent pathloss is determined from scatter plots of the received power and modeled in dB, as

$$PL(d) = PL_0 + 10n\log_{10}\left(\frac{d}{d_0}\right) + X_\sigma \tag{14}$$

where PL_0 is the pathloss at a reference distance d_0, n is the pathloss exponent and X_σ is a log-normal distributed fading with standard deviation σ. Fig. 11 shows scatter plots from all measurements. Only the MAX-Lab PP-NLOS data are sufficient to render reliable pathloss parameters, but it can be seen from the figure that the power samples from the other scenarios/measurements follow a very similar decay. The pathloss exponent for the MAX-Lab PP-NLOS is estimated to 1.1, whereas the log-normal fading has a standard deviation $\sigma = 1.1$ dB. We note that this pathloss exponent is surprisingly low, much lower than what other measurement campaigns have reported in the literature. A possible cause for the low exponent is the very rich multipath in the factory hall.

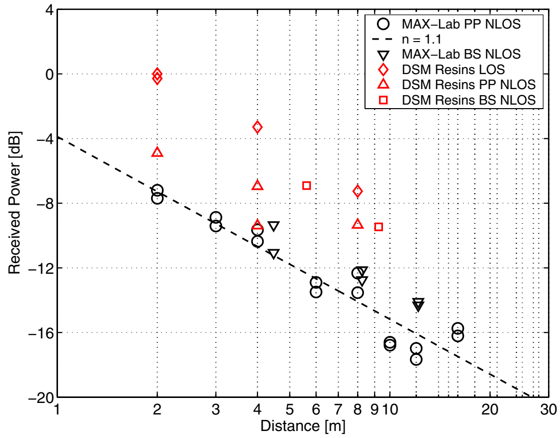

Fig. 11. Scatter plot of the received power for all measurements, normalized to the strongest value.

E. Validation of Model

To prove the validity of the model, we generate a number of impulse responses for each scenario and compare the simulation results with our measurements. Deriving 100 APDPs, each averaged from 49 individual impulse responses as given by Eqs. (5) and (6), gives a good fit for the rms delay spread. We obtain a simulated mean value of 27 ns for DSM LOS, to compare with the measured values of $28 - 38$ ns. For DSM NLOS A, simulated mean is 36 ns, whereas measured values are between $34 - 50$ ns. For MAX-Lab PP NLOS A, we obtain a simulated mean of 40 ns, to compare with the measured values $34 - 45$ ns, whereas for MAX-Lab PP NLOS B, our simulated value of 41 ns is to compare with the measured delay spreads $38 - 50$ ns.

For the energy capture by Rake receivers, the measurement bandwidth is different between the two factory halls. Therefore, our reported number of required Rake fingers is higher for the DSM hall than for MAX-Lab. Comparing the energy capture of a 5 finger Rake receiver, we find that for DSM LOS, the simulation renders a mean value of 13%, to compare with the measured values of $13 - 36\%$, whereas a simulated 20 finger Rake receiver would on average capture 31% of the energy, compared with $30 - 52\%$ in the measurements. For DSM NLOS A, the simulated mean energy capture of a 5 finger Rake is 6%, to compare with the measured $7 - 18\%$. Corresponding values for a 20 finger Rake is 16% (simulated) and $18 - 32\%$ (measured). For MAX-Lab PP-NLOS A, a simulated Rake receiver captures, on average, 16 and 39% for 5 and 20 fingers, respectively. Measured values range between

14 and 33% for a 5 finger Rake, and between 34 and 59% for a 20 finger Rake. Finally, for MAX-Lab PP-NLOS B, the simulated mean energy capture for a 5 and 20 finger Rake, respectively, is 10 and 29%, to compare with the measured values $12-17\%$ and $31-40\%$.

VII. Summary and Conclusions

We presented measurements of the ultra-wideband channel in two factory halls. The measurements cover a bandwidth from $3.1-10.6$ or $3.1-5.5$ GHz, and thus give very fine delay resolution. The main results can be summarized as follows:

- Due to the presence of multiple metallic reflectors, the multipath environments are dense; in other words, almost all resolvable delay bins contain significant energy - especially for NLOS situations at larger distances. This is in contrast to UWB office environments, as described, e.g., in [15].
- The inter-path arrival times were so small that they were not resolvable even with a delay resolution of 0.13 ns.
- For shorter distances, a strong first component exists, irrespective of whether there is LOS or not.
- For larger distances and PP NLOS scenarios, the maximum of the power delay profile is several tens of nanoseconds after the arrival of the first component. The common approximation of a single-exponential PDP does not hold at all in those cases.
- Clusters of MPCs can be observed.
- Delay spreads range from 30 ns for LOS scenarios at shorter distances to 50 ns for NLOS at larger distances.

We have also established a statistical model that describes the behavior of the channel, where it is found that the power delay profile can be well described by a generalized Saleh-Valenzuela model (with model parameters given in Table II), which is also used in the IEEE 802.15.4a channel models [21]. There are several noteworthy points:

- In contrast to the classical SV model, the ray power decay constants depend on the excess delay. This dependence is well described by a linear relationship. The decay constants vary between 0.5 and 70 ns.
- The peak cluster power can be described by an exponential function of the excess delay.
- The number of clusters varies between 4 and 6.
- The small-scale fading is well described by a Rayleigh distribution, except for the first components in each cluster, which can show a strong specular contribution.

Additionally, we found that the number of MPCs that is required for capturing 50% of the energy of the impulse response can be very high, up to 200. This serves as motivation to investigate suboptimum receiver structures that do not require one correlator per MPC, e.g., transmitted-reference schemes, [32], [33], [34], as well as noncoherent schemes. Also, the energy capture of partial Rake receivers, that match their fingers to the *first* arriving multipath components, will be highly affected in our measured NLOS scenarios, especially at larger distances.[5] This is due to the fact that the maximum of the PDP occurs some 250 taps *after* the arrival of the first MPC. Furthermore, the pronounced minimum between the LOS component and the subsequent components also reduces the energy capture of the partial Rake in LOS scenarios. We also find that a considerable percentage of the received energy lies outside a 60 ns wide window; this is important in the context of a current IEEE 802.15.3a standardization proposal, which uses OFDM with a 60 ns guard interval.

Our results emphasize the crucial importance of realistic channel models for system design. Parts of the measurements have been used as an input to the IEEE 802.15.4a channel modeling group, which (among other issues) recently have developed a channel model for industrial environments. Our measurement results thus allow a better understanding of UWB factory channels, and provide guidelines for robust system design in such environments.

[5]The overall performance, however, is determined by the combination of pathloss, amount of fading, and energy capture.

VIII. Acknowledgements

We thank DSM Resins Scandinavia for their permission to perform the measurements in their factory hall. Especially, we would like to thank Mr. Bengt-Åke Ling, Mr. Gert Wranning, and Mr. Alf Jönsson for their help and cooperation. We would also like to express gratitude to MAX-Lab for their permission to letting us perform measurements and to Mr. M. Gufran Khan and Mr. Asim A. Ashraf for their assistance during measurement campaign 3. Part of this work was financially supported by an INGVAR grant of the Swedish Strategic Research Foundation and the SSF Center for High Speed Wireless Communication.

References

[1] R. A. Scholtz, "Multiple access with time-hopping impulse modulation," in *Proc. IEEE Military Communications Conference*, vol. 2, 1993, pp. 447–450.

[2] M. Z. Win and R. A. Scholtz, "Ultra-wide bandwidth time-hopping spread-spectrum impulse radio for wireless multiple-access communications," *IEEE Trans. Commun.*, vol. 48, pp. 679–691, Apr. 2000.

[3] C. J. LeMartret and G. B. Giannakis, "All-digital PAM impulse radio for multiple-access through frequency-selective multipath," in *Proc. IEEE Global Telecommunications Conference*, 2000, pp. 77–81.

[4] M. G. diBenedetto, T. Kaiser, A. F. Molisch, I. Oppermann, C. Politano, and D. Porcino (eds.), *UWB communications systems, a comprehensive overview*. Hindawi Publishing, 2005.

[5] Federal Communications Commission, "First report and order 02-48," 2002.

[6] M. Z. Win and R. A. Scholtz, "Impulse radio: how it works," *IEEE Commun. Lett.*, vol. 2, pp. 36–38, Feb. 1998.

[7] ——, "On the robustness of ultra-wide bandwidth signals in dense multipath environments," *IEEE Commun. Lett.*, vol. 2, no. 2, pp. 51–53, Feb. 1998.

[8] ——, "On the energy capture of ultra-wide bandwidth signals in dense multipath environments," *IEEE Commun. Lett.*, vol. 2, no. 9, pp. 245–247, Sept. 1998.

[9] C. Duan, G. Pekhteryev, J. Fang, Y. Nakache, J. Zhang, K. Tajima, Y. Nishioka, and H. Hirai, "Transmitting multiple HD video streams over UWB links," in *Proc. IEEE Consumer Communications and Networking Conference*, vol. 2, Jan. 2006, pp. 691–695.

[10] A. F. Molisch, *Wireless Communications*. Chichester, West Sussex, UK: IEEE Press–Wiley, 2005.

[11] D. Cassioli, M. Z. Win, and A. F. Molisch, "The ultra-wide bandwidth indoor channel: From statistical models to simulations," *IEEE J. Sel. Areas Commun.*, vol. 20, no. 6, pp. 1247–1257, Aug. 2002.

[12] S. Ghassemzadeh, R. Jana, C. Rice, W. Turin, and V. Tarokh, "Measurement and modeling of an ultra-wide bandwidth indoor channel," *IEEE Trans. Commun.*, vol. 52, pp. 1786–1796, 2004.

[13] C.-C. Chong and S. K. Yong, "A generic statistical based UWB channel model for highrise apartments," *IEEE Trans. Antennas Propag.*, vol. 53, no. 8, pp. 2389–2399, Aug. 2005.

[14] C.-C. Chong, Y. Kim, S. K. Yong, and S. S. Lee, "Statistical characterization of the UWB propagation channel in indoor residential environment," *Wiley J. Wireless Commun. Mobile Computing*, vol. 5, no. 5, pp. 503–512, Aug. 2005.
[15] A. F. Molisch, J. R. Foerster, and M. Pendergrass, "Channel models for ultrawideband personal area networks," *IEEE Personal Commun. Mag.*, vol. 10, pp. 14–21, Dec. 2003.
[16] T. S. Rappaport, S. Y. Seidel, and K. Takamizawa, "Statistical channel impulse response models for factory and open plan building radio communication system design," *IEEE Trans. Commun.*, vol. 39, no. 5, pp. 794–807, May 1991.
[17] R. C. Qiu, "A generalized time domain multipath channel and its application in ultra-wideband UWB wireless optimal receiver design - Part II: Physics-based system analysis," *IEEE Trans. Wireless Commun.*, vol. 3, no. 6, pp. 2312–2324, 2004.
[18] J. Kunisch and J. Pamp, "Measurement results and modeling aspects for the UWB radio channel," in *IEEE Conference on Ultra Wideband Systems and Technologies Digest of Technical Papers*, 2002, pp. 19–23.
[19] A. S. Y. Poon and M. Ho, "Indoor multiple-antenna channel characterization from 2 to 8 GHz," in *Proc. Int. Conference on Communications*, May 2003.
[20] A. F. Molisch, "Ultrawideband propagation channels - theory, measurement, and modeling," *IEEE Trans. Veh. Technol.*, vol. 54, no. 5, pp. 1528–1545, Sept. 2005.
[21] A. F. Molisch et al., "IEEE 802.15.4a channel model - final report, Tech. Rep. Document IEEE 802.15-04-0662-02-004a, 2005.
[22] J. Karedal, F. Tufvesson, P. Almers, S. Wyne, and A. F. Molisch, "Setup for frequency domain ultra-wideband measurements using the virtual array principle," Dept. of Electroscience, Lund University, Sweden, Tech. Rep. ISSN 1402-8840, No. 9, Sep. 2006.
[23] T. S. Rappaport, *Wireless Communications—Principles and Practices*. Upper Saddle River, NJ: Prentice Hall, 1996.
[24] H. Krim and M. Viberg, "Two decades of array signal processing: The parametric approach," *IEEE Signal Processing Mag.*, vol. 13, no. 4, pp. 67–94, July 1996.
[25] L. J. Greenstein, V. Erceg, Y. S. Yeh, and M. V. Clark, "A new path-gain/delay-spread propagation model for digital cellular channels," *IEEE Trans. Veh. Technol.*, vol. 46, no. 2, pp. 477–485, May 1997.
[26] A. A. M. Saleh and R. A. Valenzuela, "A statistical model for indoor multipath propagation," *IEEE J. Sel. Areas Commun.*, vol. 5, no. 2, pp. 128–137, Feb. 1987.
[27] L. Vuokko, P. Vainikainen, and J. Takada, "Clusters extracted from measured propagation channels in macrocellular environments," *IEEE Trans. Antennas Propag.*, vol. 53, pp. 4089–4098, Dec. 2005.
[28] M. Toeltsch, J. Laurila, K. Kalliola, A. F. Molisch, P. Vainikainen, and E. Bonek, "Statistical characterization of urban spatial radio channels," *IEEE J. Sel. Areas Commun.*, vol. 20, pp. 539–549, Apr. 2002.
[29] J. B. Andersen and P. Eggers, "A heuristic model of power delay profiles in landmobile communications," in *Proc. URSI International Symposium on Electromagnetic Theory*, Sydney, 1992, pp. 55–57.
[30] J. Karedal, F. Tufvesson, and A. F. Molisch, *IEEE Commun. Lett.*, to be published.
[31] A. Abdi and M. Kaveh, "Performance comparison of three different estimators for the Nakagami *m* parameter using Monte Carlo simulation," *IEEE Commun. Lett.*, vol. 4, no. 4, pp. 119–121, Apr. 2000.
[32] J. D. Choi and W. E. Stark, "Performance of ultra-wideband communications with suboptimal receivers in multipath channels," *IEEE J. Sel. Areas Commun.*, vol. 20, no. 9, pp. 1754–1766, Dec. 2002.
[33] F. Tufvesson, S. Gezici, and A. F. Molisch, "Ultra-wideband communications using hybrid matched filter correlation receivers," *IEEE Trans. Wireless Commun.*, in press.
[34] T. Q. S. Quek and M. Z. Win, "Analysis of UWB transmitted reference communication systems in dense multipath channels," *IEEE J. Sel. Areas Commun.*, vol. 23, no. 9, pp. 1863–1874, Sept. 2005.

Johan Karedal received the M.S. degree in engineering physics in 2002 from Lund University in Sweden. In 2003, he started working towards the Ph.D. degree at the Department of Electroscience, Lund University, where his research interests are on channel measurement and modeling for MIMO and UWB systems. He has participated in the European research initiative "MAGNET."

Shurjeel Wyne received his B.Sc. degree in electrical engineering from UET Lahore in Pakistan, and his M.S. degree in digital communications from Chalmers University of Technology, Gothenburg in Sweden. In 2003, he joined the radio systems group at Lund University in Sweden, where he is working towards his PhD. His research interests are in the field of measurement and modeling of wireless propagation channels particularly for MIMO systems. Shurjeel has participated in the European research initiative "COST273," and is currently involved in the European network of excellence "NEWCOM."

Peter Almers received the M.S. degree in electrical engineering in 1998 from Lund University in Sweden. In 1998, he joined the radio research department at TeliaSonera AB (formerly Telia AB), in Malmö, Sweden, mainly working with WCDMA and 3GPP standardization physical layer issues. Peter is currently working towards the Ph.D. degree at the Department of Electroscience, Lund University. He has participated in the European research initiatives "COST273," and is currently involved in the European network of excellence "NEWCOM" and the NORDITE project "WILATI." Peter received an IEEE Best Student Paper Award at PIMRC in 2002.

Fredrik Tufvesson was born in Lund, Sweden in 1970. He received the M.S. degree in Electrical Engineering in 1994, the Licentiate Degree in 1998 and his Ph.D. in 2000, all from Lund University in Sweden. After almost two years at a startup company, Fiberless Society, Fredrik is now associate professor at the department of Electroscience. His main research interests are channel measurements and modeling for wireless communication, including channels for both MIMO and UWB systems. Beside this, he also works with channel estimation and synchronization problems, OFDM system design and UWB transceiver design.

Andreas F. Molisch (S'89, M'95, SM'00, F'05) received the Dipl. Ing., Dr. techn., and habilitation degrees from the Technical University Vienna (Austria) in 1990, 1994, and 1999, respectively. From 1991 to 2000, he was with the TU Vienna, becoming an associate professor there in 1999. From 2000-2002, he was with the Wireless Systems Research Department at AT&T (Bell) Laboratories Research in Middletown, NJ. Since then, he has been with Mitsubishi Electric Research Labs, Cambridge, MA, USA, where he is now Distinguished Member of Technical Staff. He is also professor and chairholder for radio systems at Lund University, Sweden.

Dr. Molisch has done research in the areas of SAW filters, radiative transfer in atomic vapors, atomic line filters, smart antennas, and wideband systems. His current research interests are measurement and modeling of mobile radio channels, UWB, cooperative communications, and MIMO systems. Dr. Molisch has authored, co-authored or edited four books, among them the recent textbook *Wireless Communications* (Wiley-IEEE Press), 11 book chapters, some 100 journal papers, and numerous conference contributions.

Dr. Molisch is an editor of the *IEEE Transactios Wireless Communications*, co-editor of recent and upcoming special issues on UWB (in *IEEE Journal on Selected Areas in Communications* and *Proc. IEEE*). He has been member of numerous TPCs, vice chair of the TPC of VTC 2005 spring, general chair of ICUWB 2006, and TPC co-chair of the wireless symposium of Globecom 2007. He has participated in the European research initiatives "COST 231," "COST 259," and "COST273," where he was chairman of the MIMO channel working group, he was chairman of the IEEE 802.15.4a channel model standardization group, and is also chairman of Commission C (signals and systems) of URSI (International Union of Radio Scientists). Dr. Molisch is a Fellow of the IEEE, an IEEE Distinguished Lecturer, and recipient of several awards.